SCIENCE CHINA
Earth Sciences

•RESEARCH PAPER•

March 2019 Vol.62 No.3: 595–608
https://doi.org/10.1007/s11430-018-9289-4

The intrinsic nonlinear multiscale interactions among the mean flow, low frequency variability and mesoscale eddies in the Kuroshio region

Yang YANG[1] & X. San LIANG[1,2*]

[1] *School of Marine Sciences, Nanjing University of Information Science and Technology, Nanjing 210044, China;*
[2] *School of Atmospheric Sciences, Nanjing University of Information Science and Technology, Nanjing 210044, China*

Received May 1, 2018; revised August 17, 2018; accepted October 24, 2018; published online January 24, 2019

Abstract Using a new functional analysis tool, multiscale window transform (MWT), and the MWT-based localized multiscale energetics analysis and canonical transfer theory, this study reconstructs the Kuroshio system on three scale windows, namely, the mean flow window, the interannual-scale (low-frequency) window, and the transient eddy window, and investigates the climatological characteristics of the intricate nonlinear interactions among these windows. Significant upscale energy transfer is observed east of Taiwan, where the mean Kuroshio current extracts kinetic energy from both the interannual and eddy windows. It is found that the canonical transfer from the interannual variability is an intrinsic source that drives the eddy activities in this region. The multiscale variabilities of the Kuroshio in the East China Sea (ECS) are mainly controlled by the interaction between the mean flow and the eddies.The mean flow undergoes mixed instabilities (i.e., both barotropic and baroclinic instabilities) in the southern ECS, while it is barotropically stable but baroclinically unstable to the north. The multiscale interactions are found to be most intense south of Japan, where strong mixed instabilities occur; both the canonical transfers from the mean flow and the interannual scale are important mechanisms to fuel the eddies. It is also found that the interannual-scale energy mainly comes from the barotropically unstable jet, rather than the upscale energy transfer from the high frequency eddies.

Keywords Kuroshio, Multiscale window transform, Canonical transfer, Multiscale energetics analysis, Multiscale interaction, Barotropic instability, Baroclinic instability

Citation: Yang Y, Liang X. 2019. The intrinsic nonlinear multiscale interactions among the mean flow, low frequency variability and mesoscale eddies in the Kuroshio region. Science China Earth Sciences, 62: 595–608, https://doi.org/10.1007/s11430-018-9289-4

1. Introduction

Kuroshio is a famous western boundary current (WBC) in the North Pacific. Originating from east of the Philippine Islands, it enters the East China Sea (ECS) along the east coast of Taiwan, and flows northeastward following the topography of the Okinawa Trough. It exits the ECS through Tokara Strait, meandering along the south coast of Japan over the Izu Ridge, and finally enters the North Pacific Ocean, becoming a zonal jet, namely, the Kuroshio Extension (Figure 1). By carrying heat northward from the tropics to midlatitude regions, Kuroshio plays a very important role in the climate system of the North Pacific. Its variabilities on different scales, which impact the local marine ecosystem and climate, have caught much attention in oceanography, thanks to the accumulating altimeter-derived and hydrographic data, as well as the availability of high-resolving regional ocean model data (e.g., Zhang et al., 2001; Waseda et al., 2002; Miyazawa et al., 2004; Wu et al., 2007; Usui et al., 2008; Zheng et al., 2011; Tseng et al., 2012; Hsin et al., 2013; Lee et al., 2013; Na et al., 2014; Soeyanto et al., 2014; Jan et al., 2017; Yuan et al., 2018).

* Corresponding author (email: san@pacific.harvard.edu)

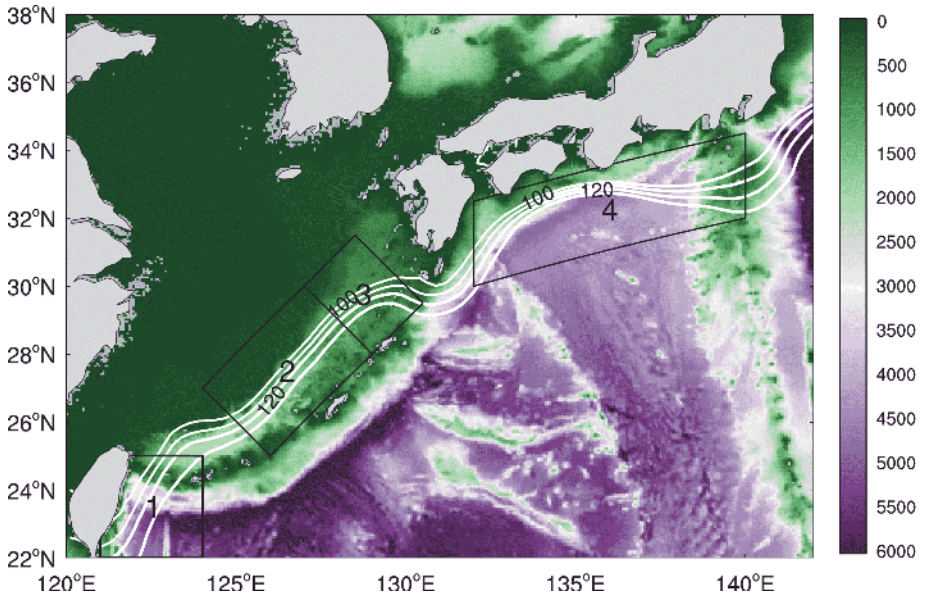

Figure 1 The bathymetry (colored; m) based on the ETOPO1 data and mean sea surface height (SSH; white contours; cm) based on the AVISO data. Only four contours (100, 110, 120 cm) of SSH, which indicate the Kuroshio axis, are plotted. The four boxes, marked as 1–4 respectively, represent the four subdomains as explained in the text.

As a strong WBC, the Kuroshio exhibits a broadband of temporal variabilities. Intense mesoscale eddy variabilities are observed in several regions of the Kuroshio system such as the waterway east of Taiwan, the ECS, and the area south of Japan (Ebuchi and Hanawa, 2000; Lee et al., 2013; Wang et al., 2014; Chang et al., 2015; Cheng et al., 2017). Mesoscale transient eddies are usually considered as high-frequency processes in the ocean, with temporal scales varying from tens to hundreds of days. In addition to these variabilities, the Kuroshio system also reveals significant low-frequency fluctuations. For instance, in several studies on the interannual variation of the Kuroshio east of Taiwan, possible relations have been proposed between such low-frequency variability and ENSO (Hwang and Kao, 2002; Shen et al., 2014), Pacific decadal oscillation (PDO; Wu, 2013), Philippines-Taiwan oscillation (PTO; Xu et al., 2017), westward propagating mesoscale eddies (Chang and Oey, 2011; Hsin et al., 2013; Chang et al., 2015; Yan et al., 2016), and local atmospheric forcing (Jia et al., 2004). The interannual variability of the Kuroshio in the ECS is also an important research topic in the past few years (Liu and Gan, 2012). Andres et al. (2009) found that the Kuroshio transport in the ECS is highly correlated with the PDO index. Using the JCOPE2 reanalysis, Soeyanto et al. (2014) suggested that the interannual modulation of the Kuroshio transport in the ECS is controlled by the combination of PDO forcing and mesoscale eddy activity southeast of Taiwan. Wang and Oey (2014) found the low-frequency fluctuations of the Kuroshio path in the ECS is better correlated with the PTO index than the PDO index. Besides, Zhang et al. (2012) identified significant interannual variation of heat transport at the PN section in the ECS and found that the overlying meridional wind anomaly is responsible for such low-frequency variability. For the Kuroshio south of Japan, it has been well established that the meandering jet undergoes a unique bimodal path transition (Usui et al., 2013), oscillating between a large meander path state and a non-large meander path state on an interannual time scale (Kawabe, 1995). This oscillation has been considered as self-sustained (Qiu and Miao, 2000), eddy driven (Miyazawa et al., 2004), and wind forced (Kurogi and Akitomo, 2003).

The above-mentioned multiscale variabilities in the Kuroshio region have a great impact on the local exchange of momentum and heat, and they may influence each other through intricate interactions. Eddy-mean flow interaction in the Kuroshio region has been an important area of research for decades. In the presence of strong velocity shear, the background flow provides energy to the eddies via baroclinic and barotropic instabilities (Waseda et al., 2002; Jia et al., 2005; Guo et al., 2018). In turn, the eddies may feedback to modulate the interannual variations of the transport and path of the Kuroshio (Hsin et al., 2013; Yin et al., 2017). This kind of interaction is a multiscale process and can be satisfactorily approached using multiscale energetic analysis (e.g., von Storch et al., 2012; Chen et al., 2014; Zemskova et al., 2015). From the outputs of a high-resolution (1/12°) ocean general circulation model, Miyazawa et al. (2004) noticed that baroclinic and barotropic instabilities play their roles at different stages of the growth of Kuroshio meander south of Japan; by diagnosing the barotropic energy transfer between the mean flow and the eddy field, Ma and Wang (2014) found that barotropic instability is responsible for the seasonal and in-

terannual eddy kinetic energy (EKE) modulations in this region.

Previous studies have suggested that oceanic processes tend to occur on a range of scales, or scale windows as called by Liang and Anderson (2007). In the case of Kuroshio system, there appear at least three scale windows, i.e., a mean flow window, an interannual-scale window, and a transient eddy window. Up to now, it is still unclear how these three scale windows may interact with each other. Also unclear is the relative contribution from the eddy-mean flow interaction and eddy-interannual interaction to the eddy growth/decay in different areas of the Kuroshio system. In this study, we will address these issues by employing a new tool of scale analysis, namely, multiscale window transform (MWT), developed by Liang and Anderson (2007), and the MWT-based localized multiscale energetics analysis and canonical energy transfer theory (Liang, 2016).

2. Methodology

Multiscale energetics analysis is a powerful tool to diagnose multiscale interactions, intrinsic instabilities and energy distributions in atmospheres and oceans. For general non-stationary multiscale processes, such as instabilities and eddy-mean flow interactions, however, the energetics studies have long been recognized as a very challenging task in geophysical fluid dynamics (GFD); even at the most basic step, i.e., at the step of how multiscale energy is expressed, there exists misconception, and conceptual mistake is frequently seen in the literature during the past decades (Liang, 2016). In this section, we give a brief introduction of multiscale energetics analysis, in the hope of clarifying some important issues which has been misunderstood during the past decades, and hence providing the community a general reference for this important topic.

2.1 Multiscale window transform

As is well known, the traditional energetics formalism based on the Reynolds mean-eddy decomposition (e.g., Lorenz, 1955; von Storch et al., 2012), in which information is lost in at least one dimension of space-time to achieve the scale decomposition, is inappropriate for the diagnosis of nonstationary processes such as instabilities. To avoid the difficulty, one usually uses filters to fulfill the decomposition. For example, a field $u(t)$ may be filtered into a background part $\overline{u}(t)$ and an eddy part $u'(t)$, where both parts are time varying. During the past decades, it has been a common practice to use $(u')^2$ as the time-varying eddy energy. This is, unfortunately, conceptually wrong. To illustrate, suppose u has a simple expansion with only two frequencies ω_0 and ω_1

$$u = \underbrace{\left(a_0\cos\omega_0 t + b_0\sin\omega_0 t\right)}_{\overline{u}(t)} + \underbrace{\left(a_1\cos\omega_1 t + b_1\sin\omega_1 t\right)}_{u'(t)}, \quad (1)$$

where $\omega_0 << \omega_1$ and the subscripts 0 and 1 hence can represent the background (low-frequency) and eddy (high-frequency) processes, respectively. For this simple example, we know the energies for the background and eddy processes should be $a_0^2 + b_0^2$ and $a_1^2 + b_1^2$, respectively, i.e., the square of the respective Fourier coefficients. They are absolutely not equal to the square of the reconstructed (filtered) fields, i.e., $[\overline{u}(t)]^2$ and $[u'(t)]^2$. That is to say, multiscale energy is a concept with the Fourier coefficients in phase space, which is related to its physical space counterpart through the Parseval equality in functional analysis (see Liang (2016) for details). In eq. (1), when $\overline{u}(t)$ is a constant, it can be easily proved that

$$a_1^2 + b_1^2 = \overline{[u'(t)]^2}, \quad (2)$$

just as the eddy energy under the Reynolds decomposition. This explains why the time averaging operator in the classical energetics formalism cannot be removed, otherwise the resulting energy (i.e., $[u'(t)]^2$) only bears the unit of energy, but does not make any sense in physics.

So it is by no means as trivial a problem as many people have been doing to obtain a physically consistent expression of time-dependent multiscale energy. In fact, this is a rather complex and fundamental problem, and has been an impossible task until filter banks and wavelets are connected (Strang and Nguyen, 1996). It has just been systematically addressed by Liang and Anderson (2007) in the development of multiscale window transform (MWT) for this very purpose.

As mentioned above, application of a traditional filter yields reconstructed fields. These reconstructed fields are variables in physical space, hence cannot be used to represent energy. Liang and Anderson (2007) realized that, just as in the Fourier transform and inverse Fourier transform, there exists a transform-reconstruction pair for a class of specially devised orthogonal filters. (Note here orthogonality is crucial; otherwise the Parseval equality does not hold and hence energy cannot even be defined.) This pair is the very MWT and its counterpart, i.e., multiscale window reconstruction (MWR). Generally, the MWR functions like what a traditional filter does, but the new transform coefficients from the MWT can be used to represent multiscale energy.

In brief, with the MWT, one can split a function space into a direct sum of several mutually orthogonal subspaces, each with an exclusive range of time scales. Such a subspace is

termed a scale window, or simply a window. In this study, we will need three scale windows, namely, the mean flow window, interannual scale window, and eddy window, which we will denote respectively by window 0, 1, and 2. For a field defined on scale windows, within the MWT framework, application of the MWT will yield MWT coefficients, e.g., $\hat{u}_n^{\sim 0}$ and $\hat{u}_n^{\sim 1}$, where $\widehat{(\cdot)}_n^{\sim \varpi}$ denotes MWT on window ϖ at time step n. The energy for each window is then proportional to the square of the coefficients, e.g., $\left(\hat{u}_n^{\sim 0}\right)^2$ and $\left(\hat{u}_n^{\sim 1}\right)^2$. Note these coefficients are by no means the filtered fields through MWR.

2.2 Canonical transfer

Within the MWT framework, Liang and Robinson (2005) developed a methodology for the study of multiscale interaction. Later on, it was refined with the introduction of the theory of canonical transfer (Liang, 2016). Hereafter we only give a brief introduction; readers are referred to Liang (2016) for more details. Consider a passive tracer T in an incompressible flow $\mathbf{u}$. The equation governing the evolution of T is

$$\frac{\partial T}{\partial t} + \nabla \cdot (\mathbf{u}T) = \ldots. \tag{3}$$

Note that processes like external source/sink and diffusion are not explicitly expressed here and all put to the right-hand side of eq. (3). Due to the existence of the nonlinear term $\nabla \cdot (\mathbf{u}T)$, multiscale interactions are expected to happen. Take MWT on both sides of eq. (3) and multiply $\hat{T}_n^{\sim \varpi}$, we have the energy equation on window ϖ

$$\frac{\partial E_n^{\varpi}}{\partial t} = -\hat{T}_n^{\sim \varpi} \nabla \cdot \widehat{(\mathbf{u}T)}_n^{\sim \varpi} + \ldots, \tag{4}$$

where $E_n^{\varpi} = \left(\hat{T}_n^{\sim \varpi}\right)^2 / 2$ is the energy on window ϖ at time step n (up to some constant). The first term of the right-hand side of eq. (4) is the nonlinear term in energy equation. It contains both transport processes due to advection, and cross-scale transfer processes. A transport process bears a divergence form in the governing equation; it integrated over a closed domain is zero, meaning that it acts as a mechanism for the redistribution of energy in the physical space. The cross-scale transfer (e.g., Lorenz, 1955; Harrison and Robinson, 1978) connects different scale processes (e.g., the mean flow and transient eddies) and is hence related to the flow instabilities. So it is very important to have the two processes separated. However, this has been a continuing challenge. As has long been recognized, the existing empirical formalisms do not have a unique separation (Holopainen, 1978; Plumb, 1983). The first attempt to tackle this problem is by Liang and Robinson (2005), within the framework of MWT; it has been satisfactorily solved just recently by Liang (2016), who proved that the inter-scale transfer is

$$\Gamma_n^{\varpi} = \frac{1}{2}\left[\widehat{(\mathbf{u}T)}_n^{\sim \varpi} \cdot \nabla \hat{T}_n^{\sim \varpi} - \hat{T}_n^{\sim \varpi} \nabla \cdot \widehat{(\mathbf{u}T)}_n^{\sim \varpi}\right]. \tag{5}$$

This transfer expression has an interesting property, namely

$$\sum_n \sum_{\varpi} \Gamma_n^{\varpi} = 0, \tag{6}$$

where the summations are over all the sampling time steps n and scale windows ϖ. Physically this means that the energy transfer is a mere redistribution of energy among the scale windows, without generating or destroying energy as a whole. This property, which is obvious by intuition, does not hold at all in the classical (empirical) formalisms. To distinguish, such as transfer is termed "canonical transfer" (see Liang (2016); previously it has also been termed "perfect transfer").

From eq. (5), one can obtain the canonical transfers of kinetic energy (KE) and available potential energy (APE) if T is replaced by velocity components and perturbation density, respectively. These two prove to precisely correspond to the classical barotropic instability and baroclinic instability in GFD (Liang and Robinson, 2007), while no spatial nor temporal averaging is taken, and hence can faithfully represent the real hydrodynamic instability processes which may be localized or intermittent in space and time. To compare canonical transfer to that resulting from the classical formalism, Liang and Robinson (2007) considered the very special case with a two-window decomposition and a zero frequency for the large scale window. In this case, the separated energy equations become

$$\frac{\partial}{\partial t}\left(\frac{1}{2}\overline{T}^2\right) + \nabla \cdot \left(\frac{1}{2}\overline{\mathbf{u}}\overline{T}^2 + \frac{1}{2}\overline{T}\,\overline{\mathbf{u}'T'}\right) = -\Gamma, \tag{7}$$

$$\frac{\partial}{\partial t}\left(\frac{1}{2}\overline{T'^2}\right) + \nabla \cdot \left(\frac{1}{2}\overline{\mathbf{u}T'^2} + \frac{1}{2}\overline{T}\,\overline{\mathbf{u}'T'}\right) = \Gamma, \tag{8}$$

where the second term of the left-hand side of eqs. (7) and (8) indicate the in-scale transport process, and Γ=(1/2) $[\overline{T}\nabla \cdot (\overline{\mathbf{u}'T'}) - \overline{\mathbf{u}'T'} \cdot \nabla \overline{T}]$ represent the canonical transfer process. The canonical transfer on the right-hand side of eqs. (7) and (8) sum to zero, satisfying the property eq. (6), and is hence a faithful representation of the energy transfer between the mean flow and eddies. By comparison, the classical energy equations for the mean and eddy fields in this case are

$$\frac{\partial}{\partial t}\left(\frac{1}{2}\overline{T}^2\right) + \nabla \cdot \left(\frac{1}{2}\overline{\mathbf{u}}\overline{T}^2\right) = -\overline{T}\nabla \cdot (\overline{\mathbf{u}'T'}), \tag{9}$$

$$\frac{\partial}{\partial t}\left(\frac{1}{2}\overline{T'^2}\right) + \nabla \cdot \left(\frac{1}{2}\overline{\mathbf{u}T'^2}\right) = -\overline{\mathbf{u}'T'} \cdot \nabla \overline{T}, \tag{10}$$

respectively. One can see that the transfer terms on the right-hand side of eqs. (9) and (10) do not cancel out:

$$\overline{T}\nabla\cdot(\overline{\mathbf{u}'T'})+\overline{\mathbf{u}'T'}\cdot\nabla\overline{T}=\nabla\cdot(\overline{T}\,\overline{\mathbf{u}'T'})\neq 0. \tag{11}$$

Note that the term $-\overline{\mathbf{u}'T'}\cdot\nabla\overline{T}$ is usually used to explain the energy transfer from the mean flow to eddies. Particularly, when T is a velocity component, this term has been interpreted as the barotropic energy transfer extracted by Reynolds stress against the mean profile (e.g., Pedlosky). Previously, Liang and Robinson (2007) illustrated, for a benchmark hydrodynamic instability model whose instability structure is analytically known, the traditional Reynolds stress extraction does not give the correct source of instability, while the canonical transfer Γ does.

2.3 Localized multiscale energy analysis

Based on MWT and the theory of canonical transfer, localized multiscale energetics can be derived conveniently from primitive equations. Consider the Navier-Stokes equations with hydrostatic and Boussinesq approximations:

$$\frac{\partial u}{\partial t}=-\nabla\cdot(u\mathbf{u})+fv-\frac{1}{\rho_0}\frac{\partial p}{\partial x}+F_u, \tag{12}$$

$$\frac{\partial v}{\partial t}=-\nabla\cdot(v\mathbf{u})-fu-\frac{1}{\rho_0}\frac{\partial p}{\partial y}+F_v, \tag{13}$$

$$0=\nabla\cdot\mathbf{u}, \tag{14}$$

$$0=-\frac{\partial p}{\partial z}-\rho g, \tag{15}$$

$$\frac{\partial\rho}{\partial t}=-\nabla\cdot(\rho\mathbf{u})-\frac{\rho_0 N^2}{g}w+F_\rho, \tag{16}$$

where $\mathbf{u}=(u,v,w)$ is the three dimensional (3D) velocity vector, f is the Coriolis parameter, g is the acceleration due to gravity, ∇ is the 3D divergence operator, F is the external forcing/dissipation, ρ is the density perturbation from the background profile $\overline{\rho}(z)$, p is the hydrostatic pressure related to ρ, and $N=\sqrt{-(g/\rho_0)(\partial\overline{\rho}/\partial z)}$ is the buoyancy frequency.

Within the MWT framework, the KE and APE on window ϖ are

$$K^{\varpi}=\frac{1}{2}\rho_0\tilde{\mathbf{u}}_H^{\varpi}\cdot\tilde{\mathbf{u}}_H^{\varpi}, \tag{17}$$

$$A^{\varpi}=\frac{1}{2}c(\tilde{\rho}^{\varpi})^2, \tag{18}$$

respectively, where $\mathbf{u}_H=(u,v)$ is the horizontal velocity vector. The coefficient $c=g^2/\rho_0N^2$ is introduced for convenience. Note that eq. (18) is the APE density under quasi-geostrophic (QG) approximation, which has been widely used in studies of mesoscale eddies in the ocean (Huang, 2005). A detailed derivation of the K^{ϖ} and A^{ϖ} equations is referred to Liang (2016); here the results are summarized:

$$\begin{aligned}&\frac{\partial K^{\varpi}}{\partial t}+\underbrace{\nabla\cdot\left[\frac{1}{2}\rho_0\widetilde{(\mathbf{u}\mathbf{u}_H)}^{\varpi}\cdot\tilde{\mathbf{u}}_H^{\varpi}\right]}_{\nabla\cdot\mathbf{Q}_K^{\varpi}}\\&+\underbrace{\nabla\cdot(\tilde{\mathbf{u}}^{\varpi}\tilde{p}^{\varpi})}_{\nabla\cdot\mathbf{Q}_P^{\varpi}}=\\&+\underbrace{\frac{1}{2}\rho_0\left[\widetilde{(\mathbf{u}\mathbf{u}_H)}^{\varpi}:\nabla\tilde{\mathbf{u}}_H^{\varpi}-\nabla\cdot\widetilde{(\mathbf{u}\mathbf{u}_H)}^{\varpi}\cdot\tilde{\mathbf{u}}_H^{\varpi}\right]}_{\Gamma_K^{\varpi}}\\&+\underbrace{(-g\tilde{\rho}^{\varpi}\tilde{w}^{\varpi})}_{b^{\varpi}}+F_K^{\varpi},\end{aligned} \tag{19}$$

$$\begin{aligned}&\frac{\partial A^{\varpi}}{\partial t}+\underbrace{\nabla\cdot\left[\frac{1}{2}c\tilde{\rho}^{\varpi}\widetilde{(\mathbf{u}\rho)}^{\varpi}\right]}_{\nabla\cdot\mathbf{Q}_A^{\varpi}}=\\&+\underbrace{\frac{1}{2}c[\widetilde{(\mathbf{u}\rho)}^{\varpi}\cdot\nabla\tilde{\rho}^{\varpi}-\tilde{\rho}^{\varpi}\nabla\cdot\widetilde{(\mathbf{u}\rho)}^{\varpi}]}_{\Gamma_A^{\varpi}}\\&+\underbrace{g\tilde{\rho}^{\varpi}\tilde{w}^{\varpi}}_{-b^{\varpi}}+F_A^{\varpi}.\end{aligned} \tag{20}$$

In eqs. (19) and (20), $\nabla\cdot\mathbf{Q}_K^{\varpi}$ and $\nabla\cdot\mathbf{Q}_A^{\varpi}$ denote the in-scale transport, i.e., the nonlocal process of energy flux divergence through advection, $\nabla\cdot\mathbf{Q}_P^{\varpi}$ is the pressure work, b^{ϖ} is the rate of buoyancy conversion which connects APE and KE on window ϖ, and F_K^{ϖ} and F_A^{ϖ}denote the forcing/dissipation processes (not explicitly expressed here). The other terms, Γ_K^{ϖ} and Γ_A^{ϖ}, and the inter-scale canonical transfers of KE and APE, respectively. They both satisfy eq. (6), indicating that they merely redistribute energy among scales.

Notice that Γ_K^{ϖ} and Γ_A^{ϖ} involve not only the transfers from outside the window but also those from within, which are irrelevant to stability/instability. We need to further differentiate them. In Liang and Robinson (2005), this is achieved through an "interaction analysis," which we will not elaborate here. For convenience, here we use the superscript $\varpi_0\to\varpi_1$ to signify the transfer from the window ϖ_0 to window ϖ_1. For instance, the canonical transfer of KE (APE) from the mean flow window ($\varpi=0$) to eddy window ($\varpi=2$) is denoted as $\Gamma_K^{0\to2}$ ($\Gamma_A^{0\to2}$). A positive $\Gamma_K^{0\to2}$ ($\Gamma_A^{0\to2}$) signifies barotropic (baroclinic) instability, which is hence called barotropic (baroclinic) transfer. Similarly, a positive $\Gamma_K^{1\to2}$ ($\Gamma_A^{1\to2}$) indicates barotropic (baroclinic) transfer from the interannual-scale window to the eddy window. The complete energy diagram based on a three-window decomposition is shown in Figure 2. This methodology is rigorous in mathematics and physics and has been applied successfully to different ocean (Yang and Liang, 2016, 2018; Yang et al., 2017) and atmosphere problems (Xu and Liang, 2017; Ma and Liang, 2017; Zhao and Liang, 2018). In this study, we only focus on the energy transfer (red arrows) and buoyancy conversion (blue arrows) processes, since they are essential to discern the intrinsic multiscale interactions in the Kur-

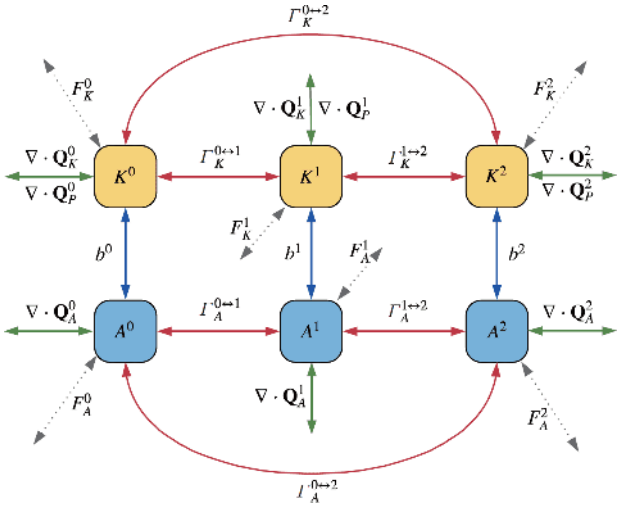

Figure 2 The energy cycle diagram for a three-window decomposition. Red arrows stand for canonical transfers, and blue ones for buoyancy conversions. Green arrows indicate nonlocal transport processes (solid) and the forcing/dissipation processes (dashed).

oshio current system. Diagnoses of the complete energy cycle is beyond the scope of the present study; we will investigate that in future studies.

3. Data

The major difficulties in performing multiscale energetics analysis with in situ observations is that observed records are usually too short and the coverage is limited. Besides, the information obtained from satellite altimetry (e.g., AVISO) is limited to the sea surface. For this reason, oceanic energetics studies are mostly based on numerical results (e.g., von Storch et al., 2012; Chen et al., 2014; Kang and Curchitser, 2015; Zemskova et al., 2015). Here we use the model outputs from "Estimating the Circulation and Climate of the Ocean" project—Phase Ⅱ (ECCO2). The ECCO2 data synthesis assimilates a large number of available satellite and in-situ data (Menemenlis et al., 2005). It is based on the Massachusetts Institute of Technology ocean general circulation model (MITgcm), which uses cube sphere grid projection with a mean horizontal resolution of 18 km. Vertically, the model has 50 levels, with resolution varying from 10 m near the sea surface to 456 m near the bottom at a maximum depth of 6150 m. The ECCO2 state estimation is based on the Green's function method to optimize a number of control parameters of the model (Menemenlis et al., 2005), including the initial temperature and salinity conditions, atmospheric surface boundary conditions, background vertical diffusivity, bottom drag, vertical viscosity, etc. (Wunsch et al., 2009). With these parameters, the model is steered forward freely, as in any ordinary model simulation. Since no data is taken in to interrupt the forward run, the state estimate is considered to be dynamically consistent (Wunsch et al., 2009; Yang et al., 2017). A more detailed description of the model configuration and the optimization scheme can be found in Menemenlis et al. (2005). Chen et al. (2014) compared the long-term mean maps of kinetic energy transfer (in the traditional sense) with the surface geostrophic currents from ECCO2 and AVISO, and found that the ECCO2 state estimate well captures the observation. We hence adopt the ECCO2 product for the purpose of this study; specifically we will use the 3-day averaged temperature and salinity (to calculate density) and the 3D velocity fields for the period of 1993–2016.

4. Scale decomposition

The approach of Reynolds mean-eddy decomposition based on time averaging, a technique widely used in previous energetics studies (e.g., von Storch et al., 2012; Chen et al., 2014; Zemskova et al., 2015), will leave low frequency (interannual to decadal) variability into the "eddy" window, resulting in spurious scale interaction results (Yang and Liang, 2016). Figure 3 shows the variance-preserved frequency spectra of KE averaged respectively over four subdomains of the Kuroshio. The KE spectra exhibit substantial multiscale variabilities in all subdomains. In general, the spectra are dominated by mesoscale variabilities with periods shorter than 1 year. In addition, the annual cycle and interannual signals are also evident in the Kuroshio system; particularly, the interannual variability is remarkably prominent in the Kuroshio south of Japan (Figure 3d). From Figure 3a–d, we can also see that the mesoscale signals show distinct spectra in different subdomains. In the region east of Taiwan and south of Japan, the periods of the mesoscale variabilities tend to be longer than 2 months; significant variabilities are even found in the band of 6 months to 1 year in the region south of Japan. In contrast, the dominant periods of mesoscale variabilities are shorter than 2 months in the northern ECS, while those to its south exhibit a broader spectrum with periods from 1 to 6 months. Based on the above, we set the cutoff period to be 384 days (=3×2^7 days, where dt=3 days is the time step size of the ECCO2 input data) to separate the high-frequency mesoscale variabilities from the low-frequency interannual fluctuations. Here the cutoff period is chosen so because, analogous to the wavelet analysis, the scale defined in MWT needs to be a power of 2; see Liang (2016) for details. We have tested the period with 192 days and the results are quantitively similar (not shown). In summary, we used the MWT to decompose the original fields into three scale windows, which we will refer to as, respectively, the mean flow window, the interannual-scale window (with periods longer than 384 days), and the mesoscale eddy window (with periods shorter than 384 days).

Notice that a scale decomposition with respect to time

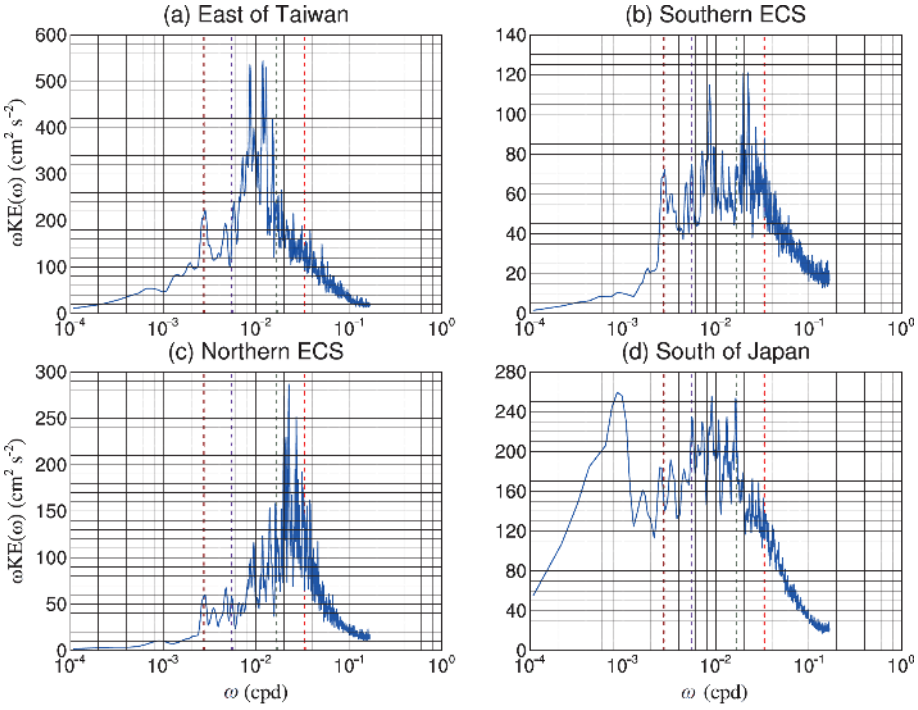

Figure 3 The variance-preserving frequency spectra of KE averaged over the four subdomains as marked in Figure 1. The dashed color lines (from right to left) in each subplot indicate the period of 1 month, 2 month, 6 month and 1 year, respectively.

inevitably allows long-lived eddy features to appear in the low-frequency field, which may leave imprints on the resulting energetics. Considering that the long-lived eddies in the Kuroshio region occur rather rarely in comparison to that of the regular high-frequency ones (Yuan and Guan, 2007; Yang et al., 2013; Cheng et al., 2014), and that we focus on the long-term mean of the multiscale energetics in this study, this should not form an issue.

5. Multiscale energy

Using eq. (17), we can compute the KE on the three windows, i.e., the mean KE (MKE, K^0), the interannual-scale KE (IKE, K^1) and the EKE (K^2). Likewise, the APE on the three windows, i.e., the mean APE (MAPE, A^0), the interannual-scale APE (IAPE, A^1) and the eddy APE (EAPE, A^2) can be obtained with eq. (18) accordingly. In this section, we examine the long-term mean spatial structures of the above six multiscale energy components.

Shown in Figure 4a–c are the horizontal distributions of the vertically averaged KE components. Generally, the three KE components exhibit clear spatial variations, with their maxima mainly confined along the Kuroshio jet. The time-mean MKE is maximized along the Kuroshio axis, and is the largest component of the three components (Figure 4a). The other component, namely, EKE, is an important quantity to measure eddy activities. The largest EKE is found east of Taiwan and south of Japan (Figure 4c). In comparison, the ECS Kuroshio region shows relatively low eddy activities; the EKE in the southern ECS is particularly weak. The third component, IKE, shows its maximum south of Japan; its value in some regions (e.g., 33°N, 137°E) even exceeds EKE. The strong interannual variability tells from an aspect that a multiscale energetics study in this region cannot be faithful without taking it into account.

Figure 4d–f show the time-mean maps of the APE on the three windows. As an important component of the total mechanical energy of mesoscale eddies (Roullet et al., 2014), the EAPE exhibits a horizontal distribution similar to that of EKE, but with much larger magnitude in the upper ocean (Figure 4f). IAPE also resembles IKE in structure. But, again, its magnitude is much larger, indicating that the interannual-scale energy is mainly stored in the form of APE (Figure 4e). Unlike MKE, the MAPE shows a different spatial distribution: it is minimized along the axis of the jet, and maximized on the two flankings. Such a MAPE pattern is due to the QG-APE used in this study (eq. (18)), which assumes that the density anomaly is a small departure from the reference state. Since the isopycnal displacements for low-frequency oscillation and/or large-scale flow may not be a small quantity at all, the QG-APE should be interpreted with caution here.

As emphasized in Section 2.1, multiscale energy is a quantity in terms of the product of transform coefficients. In this sense, the multiscale KE formalism is natural because KE takes a quadratic form. However, the local definition APE in many situations may not be quadratic (Holliday and

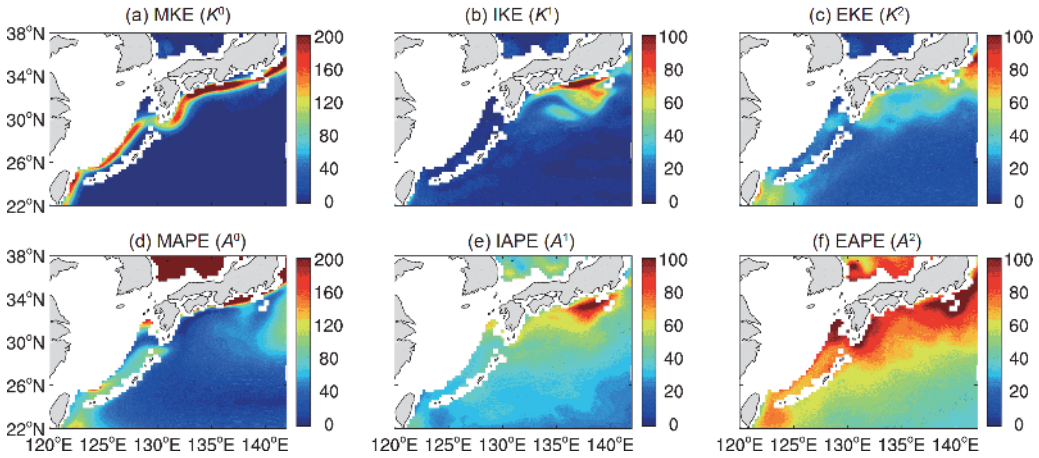

Figure 4 Temporally (1993–2016) and vertically (upper 200 m) averaged multiscale KE and APE components (J m^{-2}).

McIntyre, 1981), which raises an issue about how to handle APE in nonquadratic form in the multiscale formalism. Here we use the well-known QG-APE definition (eq. (18)), which takes a quadratic form (Liang, 2016). Up to now, the definition of APE is still an active arena of research (Tailleux, 2013). Exploration of a multiscale APE formula in nonquadratic is beyond the scope of the present study. We leave that to future studies.

Notice that the QG approximation has been found not essential to the interaction term in the APE equation. For instance, Zemskova et al. (2015) derived the mean and fluctuating APE budget equations using local definition of APE, and compared them with the ones in the QG approximation. They found that the errors in the QG approximation is only significant in high-latitude regions where local density perturbations are large due to the generation of deep waters. This might be a reason why recent energetics studies prefer to use the QG-APE (e.g., von Storch et al., 2012; Chen et al., 2014; Kang and Curchitser, 2015).

We have two observations about the above results. First, the interannual-scale window is a reservoir comparable to the other two windows, which is particularly evident in the region south of Japan. Previous studies using time mean-eddy decomposition artificially treat this part of energy as eddy energy, resulting in spurious scale interaction patterns. Second, the energy components exhibit clear streamwise variations along the Kuroshio axis. For convenience, they may be considered separately in a number of subdomains: the channel east of Taiwan, the ECS, and the region south of Japan. Since the eddy-mean flow interaction exhibits distinct directions in the northern and southern ECS (see Section 6.1), the ECS Kuroshio is further divided into the northern and southern branches. These four subdomains are marked and labeled by numbers in Figure 1. The vertical distributions of the area-mean energy densities are illustrated in Figure 5. On the whole, the MKE is the largest reservoir among the three KE components; it decays rapidly with depth. In contrast, the IKE and EKE have much smaller magnitudes. The three KE components also reveal a clear spatial variation. By observation we have MKE>EKE>IKE both along east coast of Taiwan and in the ECS (Figure 5a–c), but south of Japan, MKE>IKE>EKE (Figure 5d), indicating the strong interannual variability in this region. Different from its KE counterpart, the relative proportion of the APE presents a rather complex structure in the vertical. MAPE, IAPE and EAPE are about one order larger in magnitude than their KE counterparts, and their relative magnitude shows a complex relation in the upper 100 m for all subdomains. Note that caution should be exercised here: the density anomaly in the mixed layer generally cannot be treated as a smaller departure from the reference stratification; QG-APE could give an APE with significant error at this depth. In the deeper layers (below 200 m) of the ECS and the region east of Taiwan, the multiscale APEs rank as, from the largest to the smallest, MAPE, EAPE and IAPE (Figure 5a–c). In the subsurface south of Japan, it is evident that the value of IAPE is much larger than the other APE components (Figure 5d), indicating that the interannual variability mainly stores its energy in the form of APE.

6. Multiscale interactions

In this section, by examining the canonical transfers among the mean flow, interannual-scale and transient eddy windows, we investigate the time-mean spatial structure of the multiscale interactions in the Kuroshio region. Based on the canonical transfer theory of Liang (2016), as introduced in section 2.2, the mean-eddy, interannual-eddy and mean-interannual barotropic and baroclinic transfers can be easily obtained. Figure 6 shows the depth-averaged maps of the canonical transfers. A general observation is that all the

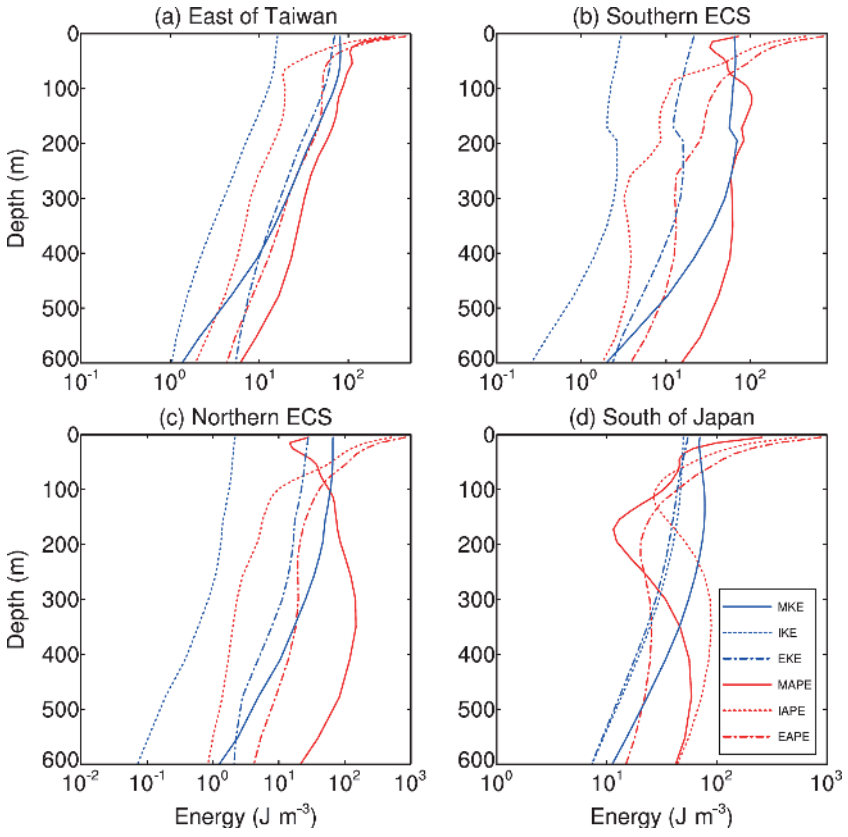

Figure 5 The vertical distribution of the time-mean multiscale energy components (J m^{-3}) averaged over the four subdomains as marked in Figure 1.

transfers are confined mainly along the jet, and are most pronounced south of Japan. Another observation is that these transfers present a clear spatial variation: high and low centers usually appear one after another along the jet axis. Note that all the energetics are temporally averaged over the 24 yr period (1993–2016) when the ECCO2 state estimates are available. We have also tried to take temporal averaging over 1994–2013 and 1995–2014, and the results are all similar. This means that the statistics are sufficient, and the climatology of the multiscale interactions obtained here are statistically meaningful.

6.1 Mean-eddy interaction

Figure 6a and 6b show the horizontal maps of vertically averaged barotropic ($\Gamma_K^{0\to2}$) and baroclinic ($\Gamma_A^{0\to2}$) transfers between the mean flow and eddies (Recall that a positive $\Gamma_K^{0\to2}$ ($\Gamma_A^{0\to2}$) indicates a transfer of KE from the mean flow to the eddy through barotropic (baroclinic) instability.) The horizontal distribution of $\Gamma_K^{0\to2}$ (Figure 6a) exhibits strong positive values in the southern ECS and off the south coast of Japan, indicating that strong EKE production through barotropic instability (i.e., MKE→EKE) occurs in these two regions. It is interesting to note that significant negative centers of $\Gamma_K^{0\to2}$, which means EKE→MKE, are distributed east of Taiwan and in the northern ECS, indicating that barotropic instability does not account for the eddy activities in these two regions. Unlike $\Gamma_K^{0\to2}$, $\Gamma_A^{0\to2}$ shows overally positive values through the Kuroshio current system; with large positive pools occupied east of Taiwan, south of the ECS and south of Japan, indicating that the MAPE reservoir releases energy to the mesoscale eddies via strong baroclinic instabilities.

Previous studies have used the Reynolds decomposition method to examine the eddy-mean flow interactions in the Kuroshio domain. For example, with a high-resolution ocean model Miyazawa et al. (2004) examined the interaction between the large Kuroshio meander and mesoscale eddies south of Japan, and found that barotropic and baroclinic instability of the meander jet are two major energy sources for the regional eddy development. Ma and Wang (2014) used satellite altimeter data to analyze the spatial distribution of barotropic energy transfer south of Japan. They found that strong barotropic instability occurs in the southern area of the Honshu Island, triggering KE transferred from the mean current to the eddies. These results are overall consistent with the present study. But it should be pointed out that our canonical transfer (eq. (5)) is fundamentally different from that with the traditional formalism (compare eqs. (7) and (8)

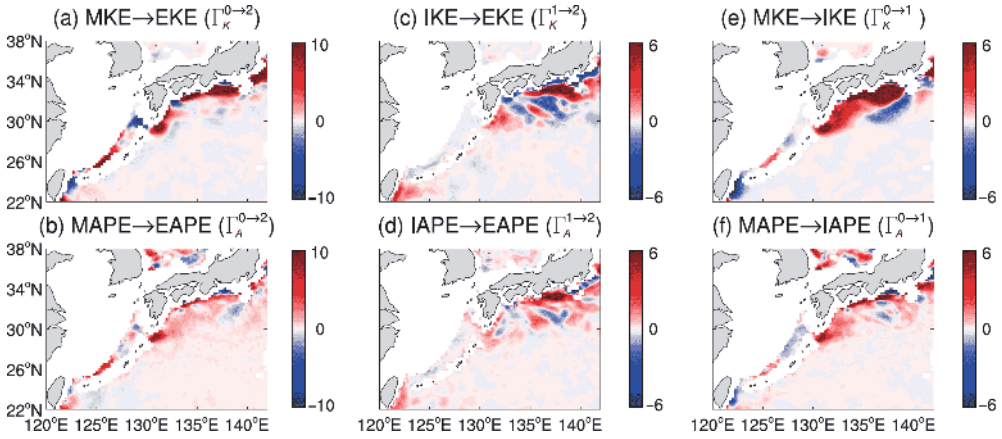

Figure 6 Temporally (1993–2016) and vertically (upper 200 m) averaged canonical transfers (10^{-4} W m^{-2}).

to (9) and (10)); the claimed instabilities in the traditional formalism are theoretically not robust.

To further illustrate the vertical structure of the energy transfers, Figure 7 displays the vertical distribution of the area-mean energetics for all the subdomains. Off the east coast of Taiwan and in the northern ECS, the area-mean $\Gamma_K^{0\to2}$ is negative and decays with depth; this inverse barotropic transfer indicates that the eddies act to drive the mean flow in these two regions (Figure 7a and 7c). In contrast, $\Gamma_K^{0\to2}$ is positive south of Japan and in the southern ECS (Figure 7b and 7d), indicating that the energy transferred from the mean to the eddy through barotropic instability is an important source for the local development of disturbances in these two subregions. Vertically, the $\Gamma_K^{0\to2}$ averaged over the southern ECS subdomain increases with depth in the upper 200 m, and decreases with depth below. The baroclinic transfer $\Gamma_A^{0\to2}$ shows positive values in all four subdomains, indicating baroclinic instabilities are occurring all over there. East of Taiwan and south of Japan, its area-mean is maximized in the surface layer, and decays dramatically with depth (Figure 7a and 7d). In the ECS, it attains its maximum in deep layers: two maxima around 120 and 350 m in the southern ECS (Figure 7b), and one maximum at 250 m in the northern ECS (Figure 7c).

6.2 Interannual variability-eddy interaction

The framework of three-window decomposition enables us to further investigate the interannual variability-eddy interaction in the Kuroshio region. From Figure 6c and 6d, it can be clearly seen that this interaction is very prominent, especially in the subdomains south of Japan and east of Taiwan. On the maps of $\Gamma_K^{1\to2}$ and $\Gamma_A^{1\to2}$, positive and negative centers are seen south of Japan, revealing a complex interaction pattern between the two scale windows. On domain average, both the barotropic and baroclinic transfers from the interannual-scale window to the eddy window are positive, indicating that forward energy cascade from the low-frequency scale acts as an important energy source to maintain the eddy development in this region (Figure 7d). Same thing happens east of Taiwan, both $\Gamma_K^{1\to2}$and $\Gamma_A^{1\to2}$ are positive, and both of them reach their maxima at the surface and gradually decay with depth (Figures 6c, 6d and 7a). This is interesting, as in the previous section, we found that barotropic instability is not the energy source for the EKE reservoir in this region. From here we know, it is the forward energy transfer from the interannual-scale variability that drives the mesoscale eddies to grow east of Taiwan.

6.3 Mean flow-interannual variability interaction

The interaction analysis further provides information for the mean flow-interannual variability interaction. Figure 6e shows the horizontal distribution of $\Gamma_K^{0\to1}$. Large and positive pools of $\Gamma_K^{0\to1}$ are found south of Japan (i.e. MKE→IKE), implying that the mean flow loses KE to the interannual-scale variability through barotropic instability, leading to the anomalously high IKE in this region. Notice that there exists a relatively weak KE transfer from the interannual-scale window back to the mean flow window. In the ECS, the interaction between these two windows is very weak. Interestingly, significant negative $\Gamma_K^{0\to1}$ is found east of Taiwan, suggesting that the mean flow draws KE from the interannual-scale variability. The horizontal distribution of $\Gamma_A^{0\to1}$ resembles that of $\Gamma_K^{0\to1}$, but with a moderate magnitude (Figure 6f). Strong baroclinic instability occurs south of Japan; energy is transferred from the MAPE reservoir to IAPE. Along the Kuroshio axis east of Taiwan, APE is transferred from the interannual-scale field back to the mean flow. Vertically, the $\Gamma_A^{0\to1}$ shows small positive values in the surface, and decreases with depth and turns negative below

50 m east of Taiwan (Figure 7a), while in the region south of Japan, it peaks at surface, and decreases gradually with depth and then increases to reach its maximum at 300 m (Figure 7d). The vertical distribution of the area-mean $I_K^{0\to1}$ shows strong negative (positive) values in the surface layer east of Taiwan (south of Japan), and decays gradually with depth (Figure 7a and 7d).

6.4 Buoyancy conversion

Buoyancy conversion (b^{ϖ}) connects KE and APE on each individual scale window ϖ. Positive b^{ϖ} indicates an energy conversion from APE to KE on window ϖ. Among its three components, the b^0 field displays a relatively complex horizontal variation, exhibiting a sequence of positive and negative centers along the stream (Figure 8a). b^0 averaged over the four subdomains are all negative (Figure 7); that is to say, the baroclinicity of Kuroshio is maintained by the MKE-to-MAPE conversion via Ekman pumping. The b^1 field shows relatively small amplitude, except for the areas south of Japan and east of Taiwan, where IKE is found to be converted to IAPE (Figure 8b). Unlike b^0 and b^1, b^2 is found to be positive (i.e., EAPE→EKE) in most of the Kuroshio region, indicating that on the whole EAPE makes an important energy source for EKE (Figure 8c). But in some particular regions there may be significant vertical structures. In the northeast area off the Taiwan coast, for example, b^2 is negative in the subsurface below 100 m (Figure 7a), indicating the EAPE reservoir receives energy from the EKE reservoir. That is to say, in these deep regions, baroclinic instability cannot account for the eddy growth. Based on this and the analysis in previous subsection, we may safely conclude that

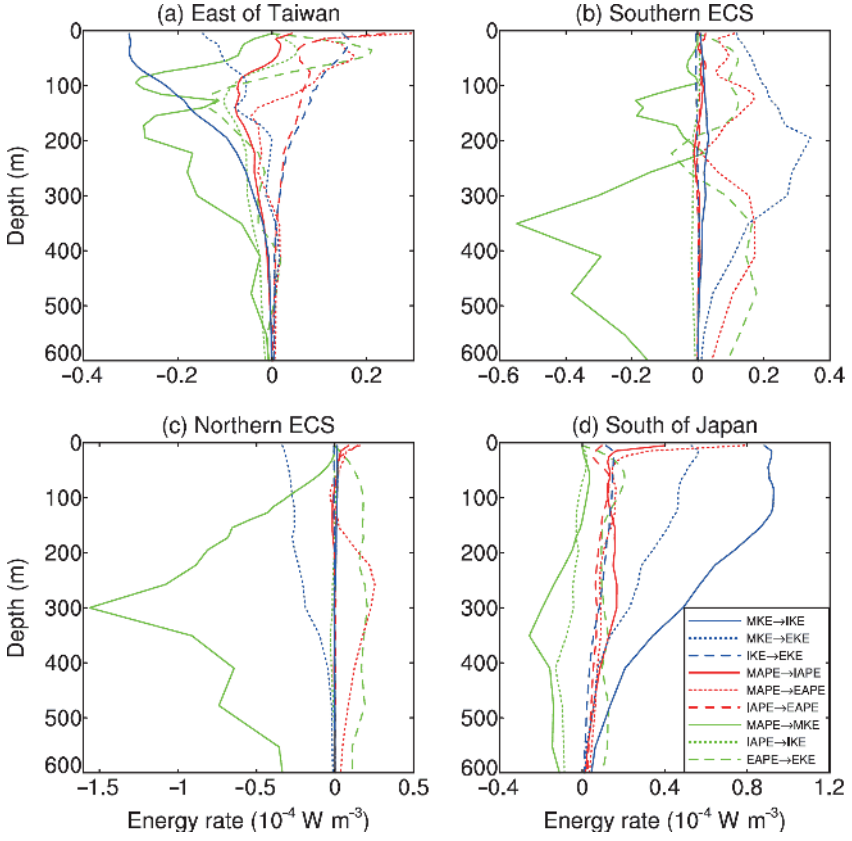

Figure 7 The vertical distribution of the time-mean multiscale energetics (10^{-4} W m^{-3}) averaged over the four subdomains as indicated in Figure 1.

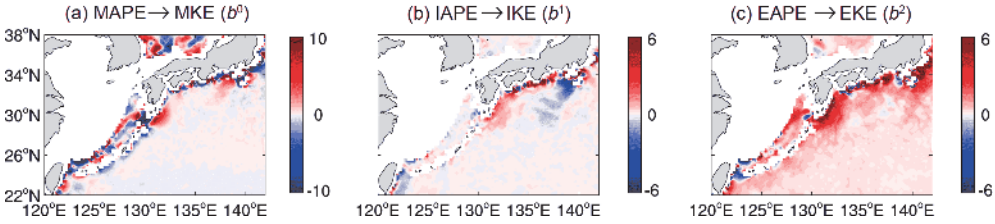

Figure 8 Temporally (1993–2016) and vertically (upper 200 m) averaged buoyancy conversions (10^{-4} W m^{-2}).

it is the forward energy cascade from the interannual scale window, rather than the barotropic energy pathway (i.e., MKE→EKE) or baroclinic energy pathway (i.e., MAPE→EAPE→EKE), that is intrinsically essential for the growth of the EKE in the Kuroshio east of Taiwan.

7. Conclusions

Using a recently developed functional analysis tool, multiscale window transform (MWT; Liang and Anderson, 2007), and the MWT-based localized multiscale energetics analysis and canonical transfer theory (Liang, 2016), this study investigates the climatological characteristics of the multiscale interactions among the mean flow, interannual fluctuation and mesoscale eddies in the Kuroshio region. We first examined the spatial distributions of the multiscale KE and APE components. It is found that the interannual variability is an energy reservoir comparable to those on the other two scale windows. Particularly, the interannual KE (IKE) and APE (IAPE) components exhibit large values in the regions south of Japan and east of Taiwan. But in previous studies based on the traditional Reynolds mean–eddy decomposition, these two components are artificially included in the EKE and EAPE reservoirs, and hence may result in spurious multiscale interactions. Following this first step we then divided the entire Kuroshio region into four subdomains, i.e., the subdomain east of Taiwan, the subdomains in the southern and northern ECS, and the subdomain south of Japan, and examined the spatial distributions and regional characteristics of the multiscale interactions. In the following, we summarize this study using the Lorenz energy cycle diagrams over the four subdomains:

(1) The subdomain east of Taiwan (Figure 9a): Strong inverse energy cascade is observed in this region. The mean flow extracts KE and APE from the interannual scale (i.e., IKE→MKE and IAPE→MAPE). The eddies are also found transferring KE back to the mean flow (i.e., EKE→MKE), indicating that the Kuroshio in this region is barotropically stable. Although the mean flow transfers energy to the EAPE reservoir through baroclinic instability (i.e., MAPE→EAPE), the EAPE is not further converted to EKE in this region. This implies that the baroclinic energy pathway is not responsible for the locally growing EKE. We further found that the energy transferred from the interannual window to the eddy window (i.e., IKE→EKE) is an important intrinsic factor for the development of the disturbances in this subdomain.

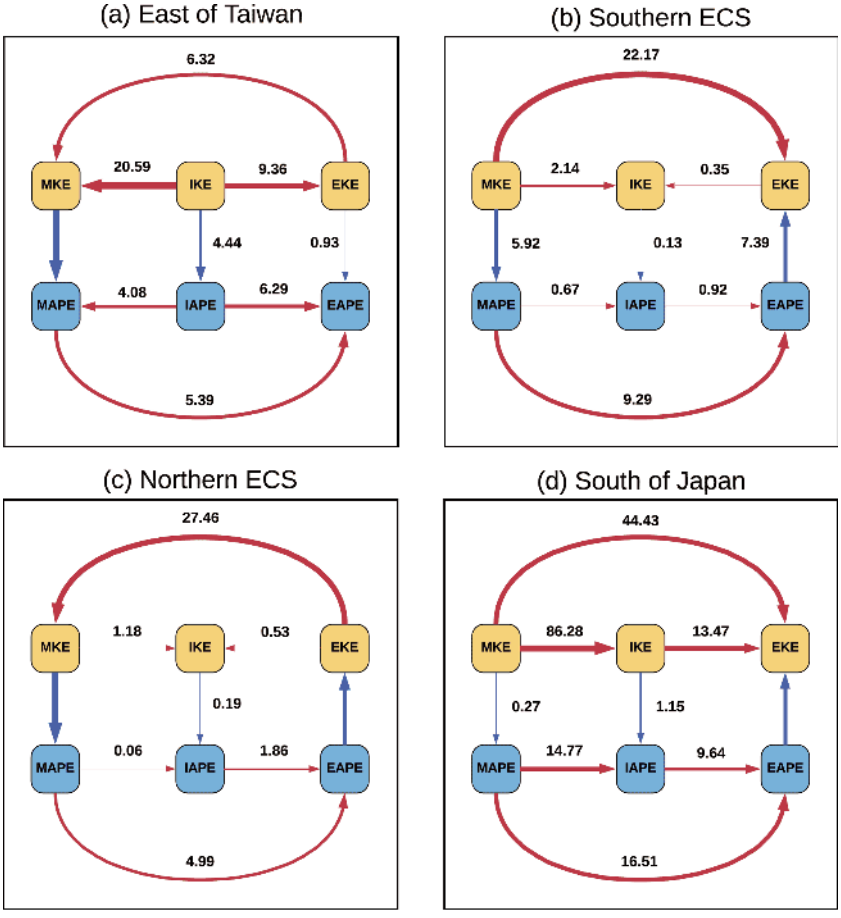

Figure 9 The volume-averaged energy diagram (as in Figure 2) for the four subdomains as indicated in Figure 1. The units are in 10^{-6} W m^{-3}.

(2) The subdomain in the southern ECS (Figure 9b): The interaction between the interannual window and the other two scale windows is weak in this region. Strong barotropic and baroclinic instabilities are observed, in contrast to the relatively low EKE level. This means that the EKE obtained via the barotropic energy pathway (MKE→EKE) and baroclinic energy pathway (MAPE→EAPE→EKE) are probably transported downstream (i.e., the northern ECS) via horizontal advection.

(3) The subdomain in the northern ECS (Figure 9c): As in the southern ECS, the interaction between the interannual window and the other two scale windows is weak. Strong inverse KE transfer (EKE→MKE) is observed in this region, suggesting that the Kuroshio is barotropically stable. Baroclinic instability is an important energy source for the local EKE (MAPE→EAPE→EKE). Another possible source might come from advection.

(4) The subdomain south of Japan (Figure 9d): This is the region where the most intense interactions among the mean flow, interannual-scale and eddy window take place. Strong barotropic and baroclinic transfers from the mean flow to eddies are observed, whereas those from the interannual scale are also important eddy energy sources. Besides fueling the eddies, the unstable mean jet also releases a large amount of energy to the interannual-scale window, implying that the strong interannual variability mainly comes from hydrodynamic instabilities (mainly barotropic instability) of the mean flow, rather than upscale transfers from the high-frequency eddies.

It should be noted that processes related to multiscale interactions are only part of the complete energy cycle. Some energy reservoirs in Figure 9 exhibit unbalanced sources or sinks. They must be balanced by other processes such as nonlocal transports by advection, pressure work, work done by wind stress and buoyancy forcing, and dissipations. Besides, the temporal (e.g., seasonal and interannual) variability of the interactions and their dynamical consequences have not been considered, but are definitely important. All these, among others, will be investigated in forthcoming studies.

Acknowledgements *This work was supported by the National Natural Science Foundation of China (Grant Nos. 41806023 and 41276032), the National Program on Global Change and Air-Sea Interaction (Grant No. GASI-IPOVAI-06), the 2015 Jiangsu Program of Entrepreneurship and Innovation Group, the Jiangsu Chair Professorship, the NUIST Startup Program (Grant No. 2017r054), and the Natural Science Foundation of the Higher Education Institutions of Jiangsu Province (Grant No. 18KJB170019).*

References

Andres M, Park J H, Wimbush M, Zhu X H, Nakamura H, Kim K, Chang K I. 2009. Manifestation of the Pacific decadal oscillation in the Kuroshio. Geophys Res Lett, 36: L16602

Chang Y L, Miyazawa Y, Guo X. 2015. Effects of the STCC eddies on the Kuroshio based on the 20-year JCOPE2 reanalysis results. Prog Oceanogr, 135: 64–76

Chang Y L, Oey L Y. 2011. Interannual and seasonal variations of Kuroshio transport east of Taiwan inferred from 29 years of tide-gauge data. Geophys Res Lett, 38: L08603

Chen R, Flierl G R, Wunsch C. 2014. A description of local and nonlocal eddy-mean flow interaction in a global eddy-permitting state estimate. J Phys Oceanogr, 44: 2336–2352

Cheng Y H, Ho C R, Zheng Q, Kuo N J. 2014. Statistical characteristics of mesoscale eddies in the North Pacific derived from satellite altimetry. Remote Sens, 6: 5164–5183

Cheng Y H, Ho C R, Zheng Q, Qiu B, Hu J, Kuo N J. 2017. Statistical features of eddies approaching the Kuroshio east of Taiwan Island and Luzon Island. J Oceanogr, 73: 427–438

Ebuchi N, Hanawa K. 2000. Mesoscale eddies observed by TOLEX-ADCP and TOPEX/POSEIDON altimeter in the Kuroshio recirculation region south of Japan. J Oceanogr, 56: 43–57

Guo J, Zhang Z, Xia C, Guo B, Yuan Y. 2018. Topographic-baroclinic instability and formation of Kuroshio current loop. Dyn Atmos Oceans, 81: 15–29

Harrison D E, Robinson A R. 1978. Energy analysis of open regions of turbulent flows—Mean eddy energetics of a numerical ocean circulation experiment. Dyn Atmos Oceans, 2: 185–211

Holliday D, McIntyre M E. 1981. On potential energy density in an incompressible, stratified fluid. J Fluid Mech, 107: 221–225

Holopainen E. 1978. A Diagnostic study of the kinetic energy balance of the long-term mean flow and the associated transient fluctuations in the atmosphere. Geophysica, 15: 125–145

Hsin Y C, Qiu B, Chiang T L, Wu C R. 2013. Seasonal to interannual variations in the intensity and central position of the surface Kuroshio east of Taiwan. J Geophys Res-Oceans, 118: 4305–4316

Huang R X. 2005. Available potential energy in the world's oceans. J Mar Res, 63: 141–158

Hwang C, Kao R. 2002. TOPEX/POSEIDON-derived space-time variations of the Kuroshio Current: Applications of a gravimetric geoid and wavelet analysis. Geophys J Int, 151: 835–847

Jan S, Mensah V, Andres M, Chang M H, Yang Y J. 2017. Eddy-Kuroshio interactions: Local and remote effects. J Geophys Res-Oceans, 122: 9744–9764

Jia Y, Liu Q, Liu W. 2005. Primary study of the mechanism of eddy shedding from the Kuroshio Bend in Luzon Strait. J Oceanogr, 61: 1017–1027

Jia Y, Liu Q, Liu W, Lin X. 2004. The Interannual Variation of the Kuroshio Transport East of Taiwan (in Chinese). Oceanol Limnol Sin, 35: 507–512

Kang D, Curchitser E N. 2015. Energetics of eddy-mean flow interactions in the Gulf Stream region. J Phys Oceanogr, 45: 1103–1120

Kawabe M. 1995. Variations of current path, velocity, and volume transport of the Kuroshio in relation with the large meander. J Phys Oceanogr, 25: 3103–3117

Kurogi M, Akitomo K. 2003. Stable paths of the Kuroshio south of Japan determined by the wind stress field. J Geophys Res, 108: 3332

Lee I H, Ko D S, Wang Y H, Centurioni L, Wang D P. 2013. The mesoscale eddies and Kuroshio transport in the western North Pacific east of Taiwan from 8-year (2003–2010) model reanalysis. Ocean Dyn, 63: 1027–1040

Liang X S. 2016. Canonical transfer and multiscale energetics for primitive and quasigeostrophic atmospheres. J Atmos Sci, 73: 4439–4468

Liang X S, Anderson D G M. 2007. Multiscale window transform. Multiscale Model Simul, 6: 437–467

Liang X S, Robinson A R. 2005. Localized multiscale energy and vorticity analysis: I. Fundamentals. Dyn Atmos Oceans, 38: 195–230

Liang X S, Robinson A R. 2007. Localized multi-scale energy and vorticity analysis: II. Finite-amplitude instability theory and validation. Dyn Atmos Oceans, 44: 51–76

Liu Z, Gan J. 2012. Variability of the Kuroshio in the East China Sea

derived from satellite altimetry data. Deep-Sea Res Part I-Oceanogr Res Pap, 59: 25–36
Lorenz E N. 1955. Available potential energy and the maintenance of the general circulation. Tellus, 7: 157–167
Ma L, Wang Q. 2014. Interannual variations in energy conversion and interaction between the mesoscale eddy field and mean flow in the Kuroshio south of Japan. Chin J Ocean Limnol, 32: 210–222
Ma J, Liang X S. 2017. Multiscale dynamical processes underlying the wintertime Atlantic blockings. J Atmos Sci, 74: 3815–3831
Menemenlis D, Fukumori I, Lee T. 2005. Using Green's functions to calibrate an ocean general circulation model. Mon Weather Rev, 133: 1224–1240
Miyazawa Y, Guo X, Yamagata T. 2004. Roles of mesoscale eddies in the Kuroshio paths. J Phys Oceanogr, 34: 2203–2222
Na H, Wimbush M, Park J H, Nakamura H, Nishina A. 2014. Observations of flow variability through the Kerama gap between the East China Sea and the Northwestern Pacific. J Geophys Res-Oceans, 119: 689–703
Oort A H, Ascher S C, Levitus S, Peixóto J P. 1989. New estimates of the available potential energy in the world ocean. J Geophys Res, 94: 3187–3200
Pedlosky J. 1987. Geophysical Fluid Dynamics. 2nd ed. New York: Springer-Verlag. 710
Plumb R A. 1983. A new look at the energy cycle. J Atmos Sci, 40: 1669–1688
Qiu B, Chen S. 2010. Eddy-mean flow interaction in the decadally modulating Kuroshio extension system. Deep-Sea Res Part II-Top Stud Oceanogr, 57: 1098–1110
Qiu B, Miao W. 2000. Kuroshio path variations south of Japan: Bimodality as a self-sustained internal oscillation. J Phys Oceanogr, 30: 2124–2137
Roullet G, Capet X, Maze G. 2014. Global interior eddy available potential energy diagnosed from Argo floats. Geophys Res Lett, 41: 1651–1656
Shen M L, Tseng Y H, Jan S, Young C C, Chiou M D. 2014. Long-term variability of the Kuroshio transport east of Taiwan and the climate it conveys. Prog Oceanogr, 121: 60–73
Soeyanto E, Guo X, Ono J, Miyazawa Y. 2014. Interannual variations of Kuroshio transport in the East China Sea and its relation to the Pacific Decadal Oscillation and mesoscale eddies. J Geophys Res-Oceans, 119: 3595–3616
Strang G, Nguyen T. 1996. Wavelets and Filter Banks. 2nd ed. Wellesley: Wellesley-Cambridge Press. 520
Tailleux R. 2013. Available potential energy and exergy in stratified fluids. Annu Rev Fluid Mech, 45: 35–58
Tseng Y H, Shen M L, Jan S, Dietrich D E, Chiang C P. 2012. Validation of the Kuroshio current system in the dual-domain Pacific Ocean Model framework. Prog Oceanogr, 105: 102–124
Usui T, McSween Jr H Y, Clark III B C. 2008. Petrogenesis of high-phosphorous Wishstone Class rocks in Gusev Crater, Mars. J Geophys Res, 113: C08047
Usui N, Tsujino H, Nakano H, Matsumoto S. 2013. Long-term variability of the Kuroshio path south of Japan. J Oceanogr, 69: 647–670
Storch J S, Eden C, Fast I, Haak H, Hernández-Deckers D, Maier-Reimer E, Marotzke J, Stammer D. 2012. An estimate of the Lorenz energy cycle for the world ocean based on the STORM/NCEP simulation. J Phys Oceanogr, 42: 2185–2205
Wang J, Oey L Y. 2014. Inter-annual and decadal fluctuations of the Kuroshio in East China Sea and connection with surface fluxes of momentum and heat. Geophys Res Lett, 41: 8538–8546
Wang X, Li C, Wang G. 2014. A study on the surface current variation within half-year time scale in active region of the Kuroshio in East China Sea (in Chinese). Acta Oceanol Sin, 36: 1–11
Waseda T, Mitsudera H, Taguchi B, Yoshikawa Y. 2002. On the eddy-Kuroshio interaction: Evolution of the mesoscale eddy. J Geophys Res, 107: 3
Wu C R. 2013. Interannual modulation of the Pacific Decadal Oscillation (PDO) on the low-latitude western North Pacific. Prog Oceanogr, 110: 49–58
Wu L, Liu Q, Hu D, Li C, Zuo J, Yu Y, Sun C, Wang Q. 2007. Variability of the subtropical gyre in North Pacific and its impacts on dynamic environment of China marginal seas (in Chinese). Adv Earth Sci, 22: 1224–1230
Wunsch C, Heimbach P, Ponte R, Fukumori I. 2009. The global general circulation of the ocean estimated by the ECCO-consortium. Oceanography, 22: 88–103
Xu F, Liang X S. 2017. On the generation and maintenance of the 2012/13 sudden stratospheric warming. J Atmos Sci, 74: 3209–3228
Xu L, Qi J, Yin B, Yang D, Chen H. 2017. Low frequency variability and machanism of the Kuroshio in the east of Taiwan (in Chinese). Acta Oceanol Sin, 39: 15–25
Yan X, Zhu X H, Pang C, Zhang L. 2016. Effects of mesoscale eddies on the volume transport and branch pattern of the Kuroshio east of Taiwan. J Geophys Res-Oceans, 121: 7683–7700
Yang G, Wang F, Li Y, Lin P. 2013. Mesoscale eddies in the northwestern subtropical Pacific Ocean: Statistical characteristics and three-dimensional structures. J Geophys Res-Oceans, 118: 1906–1925
Yang Y, San Liang X. 2016. The instabilities and multiscale energetics underlying the mean-interannual-eddy interactions in the Kuroshio extension region. J Phys Oceanogr, 46: 1477–1494
Yang Y, San Liang X, Qiu B, Chen S. 2017. On the decadal variability of the eddy kinetic energy in the Kuroshio extension. J Phys Oceanogr, 47: 1169–1187
Yang Y, Liang X S. 2018. On the seasonal eddy variability in the Kuroshio extension. J Phys Oceanogr, 48: 1675–1689
Yin Y, Lin X, He R, Hou Y. 2017. Impact of mesoscale eddies on Kuroshio intrusion variability northeast of Taiwan. J Geophys Res-Oceans, 122: 3021–3040
Yuan Y, Guan B. 2007. Overview of studies on some eddies in the China seas and their adjacent seas II. The East China Sea and the region east of the Ryukyu Islands (in Chinese). Acta Oceanol Sin, 29: 1–17
Yuan D, Hao J, Li J, He L. 2018. Cross-shelf carbon transport under different greenhouse gas emission scenarios in the East China Sea during winter. Sci China Earth Sci, 61: 659–667
Zemskova V E, White B L, Scotti A. 2015. Available potential energy and the general circulation: Partitioning wind, buoyancy forcing, and diapycnal mixing. J Phys Oceanogr, 45: 1510–1531
Zhang D, Lee T N, Johns W E, Liu C T, Zantopp R. 2001. The Kuroshio east of Taiwan: Modes of variability and relationship to interior ocean mesoscale eddies. J Phys Oceanogr, 31: 1054–1074
Zhang Q, Hou Y, Yan T. 2012. Inter-annual and inter-decadal variability of Kuroshio heat transport in the East China Sea. Int J Climatol, 32: 481–488
Zhao Y B, Liang X S. 2018. On the inverse relationship between the boreal wintertime Pacific jet strength and storm-track intensity. J Clim, 31: 9545–9564
Zheng Q, Tai C K, Hu J, Lin H, Zhang R H, Su F C, Yang X. 2011. Satellite altimeter observations of nonlinear Rossby eddy-Kuroshio interaction at the Luzon Strait. J Oceanogr, 67: 365–376

(Responsible editor: Lixin WU)